Nigerian Journal of Environmental Sciences and Technology
(NIJEST)
www.nijest.com
ISSN (Print): 2734-259X | ISSN (electronic): 2734-2603
Vol 9, No. 2 October 2025, pp 138 - 148

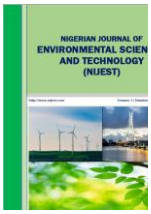

Numerical Model for Predicting the Flexural Performance of Plate-Bonded Retrofitted RC Beams

Francis, E. W.[1], * Auta, S.M.[1], Aguwa J.I[1]. and Abdullahi, A.[1]
[1,] Department of Civil Engineering, Federal University of Technology, Minna, Nigeria
Corresponding Author: *francisebitei@yahoo.com

https://doi.org/10.36263/nijest.2025.02.68

ABSTRACT

This study presents the development of a numerical model for predicting the flexural behaviour of reinforced concrete (RC) beams strengthened with externally bonded steel plates. The objective is to improve understanding of the structural response and effectiveness of plate-bonding retrofitting techniques, particularly with respect to flexural capacity, deformation behaviour, and failure mechanisms. A finite element model (FEM) was developed using an eight-noded interface element to represent the steel to adhesive to concrete interface, whose thickness is assumed negligible. The formulation is based on isoparametric elements with parabolic shape functions and a two-point Gaussian integration scheme. The numerical simulations accurately capture the load–deflection response, ultimate load capacity, and failure modes of plate-strengthened RC beams. Comparison with experimental results shows strong agreement, with predicted ultimate loads deviating by less than −3.27% to +6.0% from measured values across all specimens. Beams strengthened with relatively thin steel plates ($t \leq 3$ mm) exhibited conventional flexural failure typical of under-reinforced RC beams, whereas increasing the plate thickness beyond 3 mm resulted in a transition to bond-controlled failure modes, including plate debonding and interface-induced cracking. This transition highlights the dominant influence of plate thickness on the interaction between flexural capacity enhancement and bond performance. Statistical validation was performed using Analysis of Variance (ANOVA) based on a linear regression model at a 95% confidence level. The computed F-value of 62.5 exceeds the critical value of 18.51, confirming a statistically significant relationship between experimental and numerical results. The coefficient of determination (R^2) of 0.969 indicates that the FEM explains 96.9% of the variation in experimental data, while a correlation coefficient of 0.9844 demonstrates excellent predictive accuracy. The proposed model provides a reliable tool for predicting flexural behaviour and failure mode transition in plate-bonded RC beams.

Keywords: Numerical, steel plate, Epoxy, Flexure, Model, Strengthening

1.0. Introduction

The structural performance of reinforced concrete (RC) beams plays a pivotal role in maintaining the overall integrity and safety of buildings and civil infrastructure (Hu et al., 2022; Di Carlo et al., 2023). Over their service life, RC beams are subjected to a range of deleterious influences including increased operational loads, progressive material degradation, and exposure to aggressive environmental conditions which cumulatively diminish their strength and durability (Al Nuaimi et al., 2022; Rincon et al., 2024). In response, retrofitting strategies are frequently employed to rehabilitate or enhance the load-bearing capacity of such deteriorated elements, with plate bonding emerging as one of the most prevalent and effective techniques (Raza et al., 2019; Siddika et al., 2020; Gkournelos et al., 2021).

Plate bonding entails the application of externally bonded reinforcements, commonly in the form of steel or fiber-reinforced polymer (FRP) plates, to the tensile face of RC beams to improve their flexural strength and stiffness (Siddika et al., 2020; John et al., 2022; Askar et al., 2022). This method offers multiple advantages, including minimal self-weight addition, ease of installation, and a substantial enhancement in structural performance (Irandegani et al., 2022; Firoozi et al., 2024; Sara-Simon et al., 2024). Nevertheless, the efficacy of such retrofitting systems is significantly influenced by several parameters most notably, the bond characteristics at the plate–concrete interface, plate thickness, adhesive properties, and applied loading conditions (Goswami et al., 2019; Hassan et al., 2019; Cao et al., 2022).

Given the complexity of these interacting variables, the accurate prediction of flexural behavior in retrofitted RC beams has become an area of intensive research (Vu et al., 2022; Omar et al., 2023). Although experimental investigations provide reliable insights (Rezaee et al., 2020), they are often constrained by high costs, time requirements, and scalability limitations. Consequently, numerical modeling has gained prominence as a powerful analytical alternative, offering the capacity to simulate intricate structural phenomena and elucidate underlying failure mechanisms.

Despite substantial progress in computational modeling, significant challenges remain particularly in simulating the nuanced material interactions and bond–slip behaviors inherent in plate-bonded retrofitted systems (Heidarzadeh, 2022; Dooshabi & Najafgholipour, 2024). Most existing numerical models either idealize the plate–concrete interface as perfectly bonded or employ simplified contact assumptions, thereby limiting their ability to accurately capture failure mode transitions and load-transfer mechanisms. Such simplifications often lead to discrepancies between predicted and experimental responses, especially for beams strengthened with varying plate thicknesses and adhesive layers. As a result, observable deviations from experimental outcomes have been reported in the literature (Bahraq et al., 2021; Amini et al., 2022).

Furthermore, while finite element formulations incorporating Jacobian matrices and isoparametric elements are well established, their application in modeling the steel to adhesive to concrete interface has not been sufficiently refined to account for thickness-dependent failure mechanisms and interfacial stress redistribution. This represents a critical research gap, as the influence of plate thickness on failure mode transition and numerical to experimental agreement remains inadequately quantified.

Accordingly, the present study endeavours to develop a robust numerical model capable of precisely predicting the flexural response of plate-bonded RC beams. Unlike existing approaches, the proposed framework explicitly addresses the limitations of simplified interface modeling by incorporating a refined interface representation that captures bond interaction effects associated with different plate thicknesses. The model leverages advanced computational techniques, including Jacobian matrix-based formulations, and is validated against empirical data to ensure predictive reliability. By quantifying both failure mode transitions and the degree of agreement between numerical predictions and experimental results, the study establishes a clearer link between modeling assumptions and structural response. The outcome is expected to provide a valued analytical tool for optimizing retrofitting strategies, enhancing structural safety, and extending the operational lifespan of RC beam elements.

2.0 Methodology

2.1. Development of Finite Element Model of Steel Glue RC Bea

This section explains the development of a finite element model, built on concepts originally introduced by Bimal & Hiroshi (2002). Given the negligible thickness of the interface, an eight-noded element, illustrated in Figure 1(a), was considered adequate to represent the steel-glue-concrete interface.

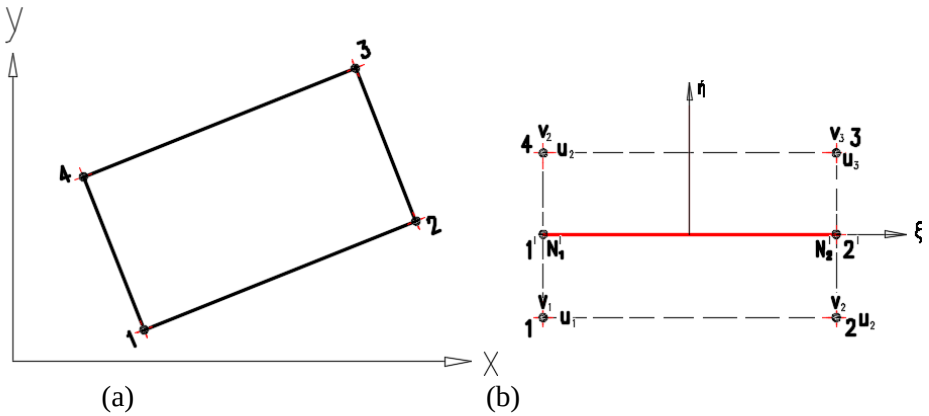

(a) (b)

Figure 1: (a) Steel-glue concrete interface element; (b) Formulation of a glued interface element

By introducing equivalent pseudo-nodes 1' and 2' (refer to Figure 1(b)), an iso-parametric formulation with parabolic shape functions could be implemented. The element employed a two-point Gaussian integration rule for its formulation.

2.1.2 Stress- strain relations

The strains in the glue element can be written as

$$\varepsilon = \begin{bmatrix} \varepsilon_\xi \\ \varepsilon_\eta \\ \gamma_{\xi\eta} \end{bmatrix} = \begin{bmatrix} \dfrac{\delta u}{\delta \xi} \\ \dfrac{\delta v}{\delta \eta} \\ \dfrac{\delta u}{\delta \eta} + \dfrac{\delta v}{\delta \xi} \end{bmatrix} \quad (1)$$

The strain ε_x along the x-direction may be approximated as

$$\varepsilon_\xi = \frac{\delta u}{\delta \xi} \quad (2)$$

Shape functions are interpolation functions that establish a relationship between the variables within a finite element and their values at the element's nodes. These nodal values are determined by solving the problem using finite element methods.

In general, we may write:

$$u(\xi) = \sum_i N_i(\xi) u_i = \boldsymbol{N} u \quad (3)$$

Where;

u(ξ) is the function under investigation (for example displacement field)

N(ξ) is the shape functions matrix

$$u = \begin{bmatrix} u_1 \\ u_2 \\ u_3 \\ u_4 \\ . \\ . \\ u_n \end{bmatrix} \; is\ the\ vector\ of\ unknowns\ in\ the\ nodes(for\ example: displacement)$$

Substituting equation 3 into 2, we have,

$$\varepsilon_\xi = \frac{\delta u}{\delta \xi} = \frac{\delta}{\delta \xi} \sum_{i=1}^{2} N_i'(\xi) \breve{u}_i = \sum_{i=1}^{2} \frac{dN_i'(\xi)}{d\xi} \breve{u}_i, \quad (4)$$

Here, $N_i = N_i(\xi)$ represent the shape functions at the three equivalent nodal points 1′and 2′ as depicted in Figure 1, while u_i denote the average nodal displacements along the line n = 0. Equation (4) can thus be expressed in terms of the element's nodal displacements, u_i.

$$\varepsilon_\xi = \frac{dN_1'}{d\xi}\left(\frac{u_1 + u_4}{2}\right) + \frac{dN_2'}{d\xi}\left(\frac{u_2 + u_3}{2}\right) \quad (5)$$

The strain in the normal direction ε_n. is given by

$$\varepsilon_n = \frac{\delta v}{\delta \eta} \quad (6)$$

and can be stated in terms of nodal normal strains as

$$\varepsilon_\eta = \sum_{i=1}^{2} N_i'(\xi)\left(\frac{\delta v}{\delta n}\right)_i = \sum_{i=1}^{2} N_i'(\xi)\left(\frac{\Delta v}{t}\right)_i = \frac{1}{t}[N_1'(v_4 - v_1) + N_2'(v_3 - v_2)] \quad (7)$$

where t is the element thickness. The shear strain $\gamma_{\xi\eta}$ is approximated as

$$\gamma_{\xi\eta} = \frac{\delta u}{\delta \eta} + \frac{\delta v}{\delta \xi} = \sum_{i=1}^{2} N_i'(\xi)\left(\frac{\delta u}{\delta \eta}\right)_i + \sum_{i=1}^{2} \frac{dN_i'(\xi)}{d\xi}\breve{v}_i$$

$$\gamma_{\xi\eta} = \frac{1}{t}[N_1'(u_4 - u_1) + N_2'(u_3 - u_2)] + \left[\frac{dN_1'}{d\xi}\left(\frac{v_1 + v_4}{2}\right) + \frac{dN_2'}{d\xi}\left(\frac{v_2 + v_3}{2}\right)\right] \quad (8)$$

Substituting Equations (5), (7) and (8) in Equation (1) we obtain,
The above equation can be written as

$$\varepsilon = [\mathbf{B}][v] \quad (9)$$

$$\varepsilon = \begin{bmatrix} \frac{1}{2}\frac{dN_1'}{d\xi} & 0 & \frac{1}{2}\frac{dN_2'}{d\xi} & 0 & \frac{1}{2}\frac{dN_2'}{d\xi} & 0 & \frac{1}{2}\frac{dN_1'}{d\xi} & 0 \\ 0 & -\frac{N_1'}{t} & 0 & -\frac{N_2'}{t} & 0 & \frac{N_2'}{t} & 0 & \frac{N_1'}{t} \\ -\frac{N_1'}{t} & \frac{1}{2}\frac{dN_1'}{d\xi} & -\frac{N_2'}{t} & \frac{1}{2}\frac{dN_2'}{d\xi} & \frac{N_2'}{t} & \frac{1}{2}\frac{dN_2'}{d\xi} & \frac{N_1'}{t} & \frac{1}{2}\frac{dN_1'}{d\xi} \end{bmatrix} \begin{bmatrix} u_1 \\ v_1 \\ u_2 \\ v_2 \\ u_3 \\ v_3 \\ u_4 \\ v_4 \end{bmatrix}$$

$$B = \begin{bmatrix} \frac{1}{2}\frac{dN_1'}{d\xi} & 0 & \frac{1}{2}\frac{dN_2'}{d\xi} & 0 & \frac{1}{2}\frac{dN_2'}{d\xi} & 0 & \frac{1}{2}\frac{dN_1'}{d\xi} & 0 \\ 0 & -\frac{N_1'}{t} & 0 & -\frac{N_2'}{t} & 0 & \frac{N_2'}{t} & 0 & \frac{N_1'}{t} \\ -\frac{N_1'}{t} & \frac{1}{2}\frac{dN_1'}{d\xi} & -\frac{N_2'}{t} & \frac{1}{2}\frac{dN_2'}{d\xi} & \frac{N_2'}{t} & \frac{1}{2}\frac{dN_2'}{d\xi} & \frac{N_1'}{t} & \frac{1}{2}\frac{dN_1'}{d\xi} \end{bmatrix} \quad (10)$$

$$v = \begin{bmatrix} u_1 \\ v_1 \\ u_2 \\ v_2 \\ u_3 \\ v_3 \\ u_4 \\ v_4 \end{bmatrix} \quad (11)$$

Where:
B is the strain matrix and v is the displacement vector
Ni are the parabolic shape functions given by equations (12) and (13)

2.1.3 Shape functions

The shape functions can be defined as:

$$N_k = \sum \frac{\xi - \xi_m}{\xi_k - \xi_m}, \quad therefore,$$

$$N_1 = \frac{\xi - \xi_2}{\xi_1 - \xi_2} = \frac{\xi - 1}{-1 - 1}$$

$$N_1 = \frac{1}{2}(1-\xi) \tag{12}$$

$$N_2 = \frac{\xi - \xi_1}{\xi_2 - \xi_1} = \frac{\xi + 1}{1 + 1}$$

$$N_2 = \frac{1}{2}(1+\xi) \tag{13}$$

2.2. Material and cracking behaviour of the interface

The material properties utilized in this study were adopted from the work of Ziraba and Baluch (1995). Their research provided comprehensive data on the mechanical characteristics and behavioral responses of materials commonly used in reinforced concrete structures. Specifically, the study referenced values such as the modulus of elasticity, Poisson's ratio, compressive strength, tensile strength, and stress-strain relationships, which are critical for accurate structural modeling and analysis. The adoption of these established material properties ensured consistency with validated experimental data and facilitated a reliable comparison with previous studies in the field of concrete mechanics and structural engineering.

2.3. Beams investigated

The finite element model developed for a steel-retrofitted reinforced concrete beam with varying external steel plate thicknesses, as detailed in Section 2, was solved using MATLAB. The model was validated by comparing its numerical results with experimental data from externally reinforced RC beams reported by Jones et al. (1982). The beams were discretized as shown in Figure 2, with a load increment of 1 kN applied at each step until failure. Referring to beams from Jones et al. (1982), Beam URB1 is an under-reinforced concrete beam without any external steel plate as shown Figure 3. It has enough shear reinforcement to ensure failure occurs through ductile flexure. Beams URB2, URB3, and URB4 are comparable to URB1 but include external steel plate with thicknesses of 1.5 mm, 3 mm, and 5 mm, respectively. In all these beams, the glue layer used to bond the steel plates is consistently 3 mm thick.

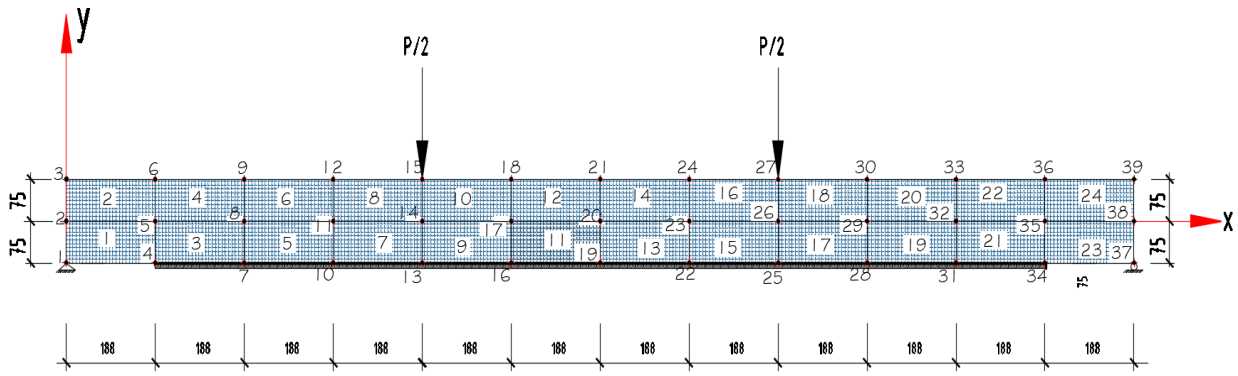

Figure 2: Discretized beam

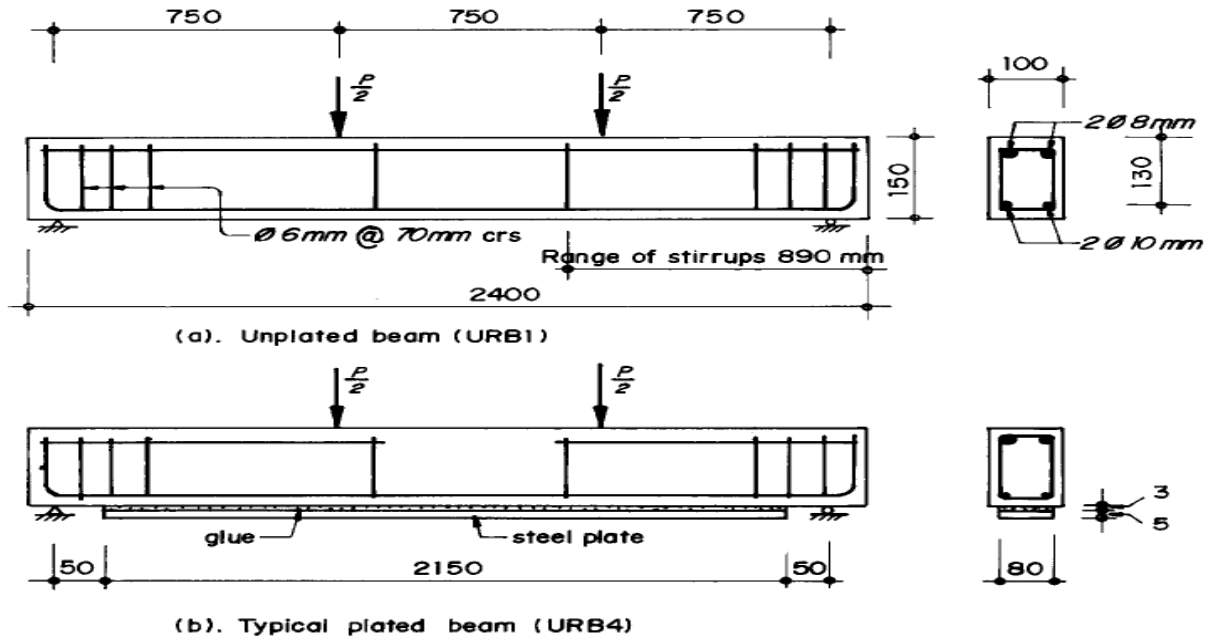

Figure 3: Details of reinforced concrete beam investigated

The material properties used in the model match those reported in the experimental study Jones et al. (1982). However, for concrete, the cylinder compressive strength (fc′) was assumed to be 85% of the cube compressive strength given in the study, as stated by Ziraba and Baluch (1995). Additional parameters required for the concrete material model are given above.

For the internal reinforcing steel and stirrups, the elastic modulus (Es) was set to 200 GPa, the yield stress (σy) to 530 MPa, and the plastic modulus (H′) to 200 MPa. The external steel plate had properties of Ep =200 GPa, H′= 200 MPa, Poisson's ratio (v) of 0.3, and yield stress (σ_y=240 MPa. The properties of the steel-glue-concrete interface used in the numerical model were Ziraba and Baluch (1995).

3.0 Results and Discussion

The finite element developed model in this study was solved using MATLAB. The model was validated by comparing its numerical results with experimental data from externally reinforced RC beams reported by Jones et al. (1982). This section provides a detailed comparison, covering ultimate loads, deflections and stress distributions, along with a discussion of the observed failure modes.

3.1. Jones et al. (1982) Experimental Results and Finite Element Model

3.1.1 Ultimate Failure Load

Table 1 shows experimental results of Jones et al. (1982) and the finite element model (FEM). Results show a strong correlation, with slight variations across all beam configurations. The unstrengthened beam (U-RB1) had an experimental ultimate failure load of 28 kN, while the FEM predicted 28.7 kN, showing a negligible 2.5% difference, validating the accuracy of the model. For U-RB2, the experimental failure load was 40 kN, while the FEM slightly overestimated it at 42.5 kN (6.25% difference).

U-RB3 showed a minor FEM underestimation of 3.27% (55 kN vs. 53.2 kN), confirming that increasing the steel plate thickness enhances load capacity. U-RB4 had a 57.5 kN experimental failure load, while the FEM overestimated at 60.4 kN (5.04% difference), suggesting that material properties and bond conditions influence actual failure. The results demonstrate that increasing the steel plate thickness improves ultimate failure load, but with diminishing returns; comparing U-RB2 to U-RB3, the failure load increased by 37.5% experimentally and 25.2% in FEM, while increasing the plate thickness to 5.0 mm (U-RB4) resulted in only a 4.5% improvement over the 3.0 mm case. This indicates that beyond a certain thickness, additional gains are minimal, making optimization more critical than simply maximizing thickness. General, the FEM results

closely align with experimental data (within 6% deviation), confirming its reliability in predicting structural performance.

Table 1: Failure Load of the Beams

Beam Configuration	Adhesive thickness (mm)	External Steel Plate thickness (mm)	**Ultimate failure Load**	
			Experimental (Jones et al., 1982) (kN)	**Finite element model (kN)**
U-RB1	-	-	28	28.7
U-RB2	3	1.5	40	42.5
U-RB3	3	3.0	55	53.2
U-RB4	3	5.0	57.5	60.4

Analysis of Variance (ANOVA) was conducted using a linear regression model to determine whether there is a statistically significant difference between the experimental and finite element model (FEM) results at a 95% significance level ($\alpha = 0.05$). The data presented in Table 2 shows that the computed F-value is 62.5. The statistical table F-value for (1, 2) degrees of freedom at a 0.05 significance level is 18.51. Given that the computed F-value (62.5) is greater than the table value (18.51), we reject the null hypothesis and accept the alternative hypothesis.

This confirms the presence of a linear relationship between the experimental and finite element model values. The coefficient of determinant, R2 was calculated to be 0.969, which means that the finite element model explains 96.9% variation in the experimental results when compared to the total variation. The correlation coefficient was computed to be 0.9844. *Comparison with experimental results shows strong agreement, with predicted ultimate loads deviating by less than −3.27% to +6.0% from measured values across all specimens. Beams strengthened with relatively thin steel plates (t□ ≤ 3 mm) exhibited conventional flexural failure typical of under-reinforced RC beams, whereas increasing the plate thickness beyond 3 mm resulted in a transition to bond-controlled failure modes, including plate debonding and interface-induced cracking*

Table 2: ANOVA table

Source of variation	**Degree of freedom**	**Sum of squares**	**Mean sum of square**	**F-ratio**
Due to regression	1	575.2	575.2	62.5
Due to Error	2	18.4	9.2	
Total	3	593.6		

3.1.3. Load-deflection Response

In investigating the behavior of RC beams, the load-deformation response is a crucial tool. Mukhopadhyaya & Swamy (1999) recommended considering deformation as a key criterion for assessing ductility in strengthened concrete beams, as these beams generally lack a clear yield point.

Figure 4 shows the load–deflection graph which illustrates the stiffness and ductility behavior of four reinforced concrete beams (RB1 to RB4) under both experimental and numerical modelling conditions. Stiffness, indicated by the slope of the initial portion of each curve, increases progressively from RB1 to RB4. ExpU-RB4 and modelU-RB4 show the steepest initial slopes, indicating the highest stiffness and load-carrying capacity, while ExpU-RB1 and modelU-RB1 exhibit the lowest stiffness. The modelled curves generally display slightly higher stiffness than their experimental counterparts due to idealized boundary conditions and material properties used in simulations. This variation in stiffness can be attributed to differences in concrete composition, reinforcement detailing, and possibly the presence and position of service ducts, which influence the effective cross-section and structural response.

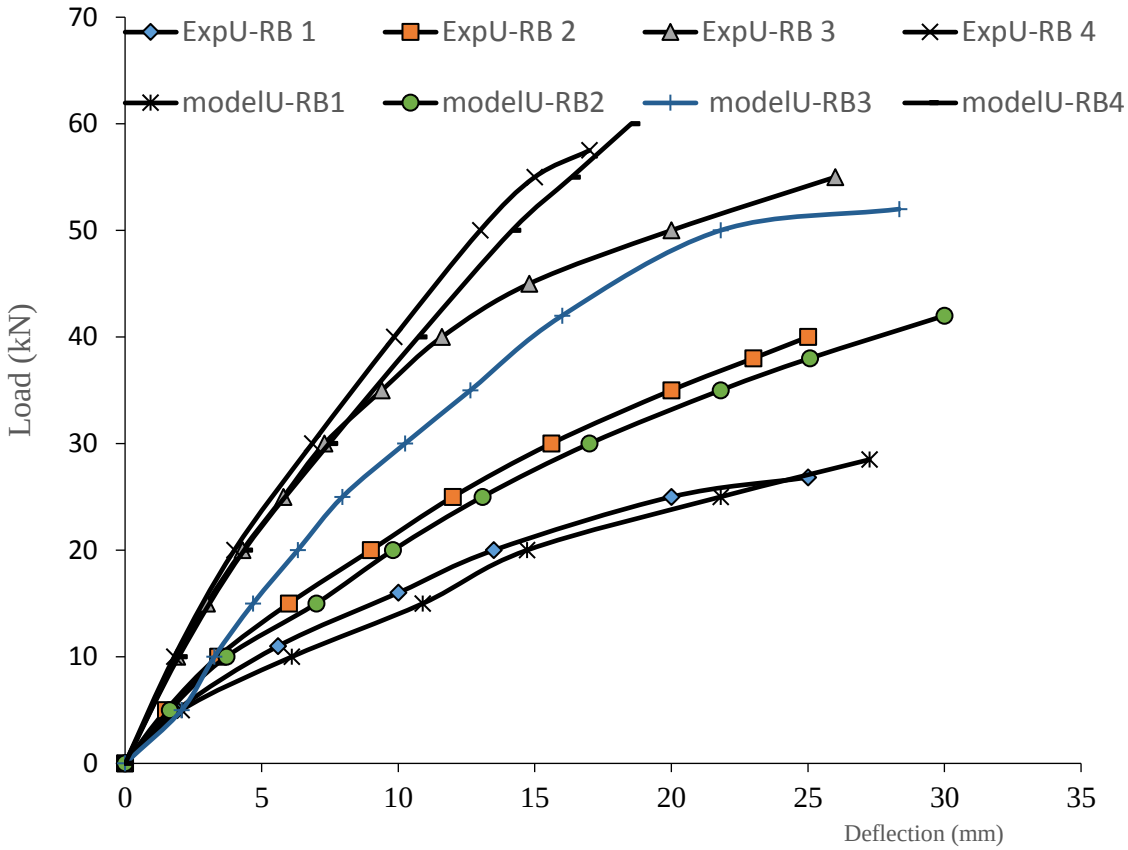

Figure 4: Load-deflection response

In terms of ductility, which reflects the beam's ability to undergo large deflections before failure, RB1 exhibits the highest ductility, followed by RB2 and RB3, while RB4 shows the lowest ductility. This inverse relationship between stiffness and ductility demonstrates a typical structural trade-off as beams become stiffer and stronger (e.g., RB4), they tend to become less ductile and more brittle. The higher ductility of RB1 may be due to a more flexible mix or configuration that allows more deformation post-yield. The modelled results also tend to predict slightly less ductility than the experimental results, again due to the simplifications in numerical models. Overall, the graph highlights the need to balance stiffness and ductility in structural design to ensure both strength and resilience under load.

3.1.4 Stress distribution

Figures 5 and 6 illustrate the distribution of tensile stress in both the internal reinforcing steel and the external plate for beams U-RB2, U-RB3, and U-RB4 under ultimate load conditions, as predicted by the finite element model. In the case of beam U-RB2 and U-RB3, both the internal reinforcement and the externally bonded plate have reached their respective yield points, indicating a typical flexural failure mechanism without any premature plate separation. This suggests effective stress transfer and composite action between the reinforcement and concrete. Figures 4 and 5 show the stress distribution along the beam length for an external steel plate and an internal steel bar. The internal steel bar experiences significantly higher stress, peaking at around 500 MPa in the central region, while the external steel plate reaches a much lower maximum stress of approximately 200 MPa.

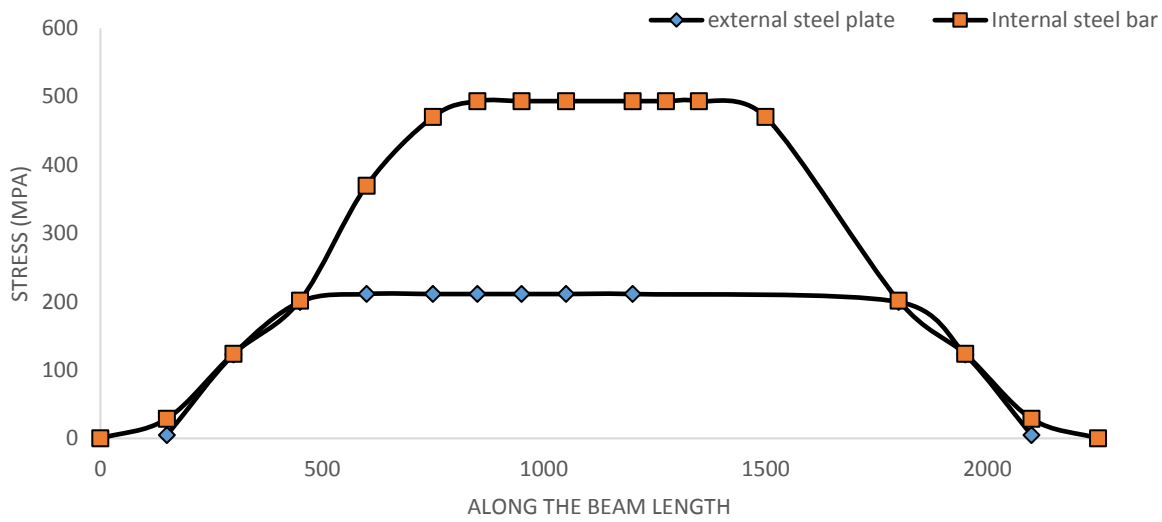

Figure 5. Normal stresses in external plate and internal main steel for beam URB2 at a load of 42.5 kN

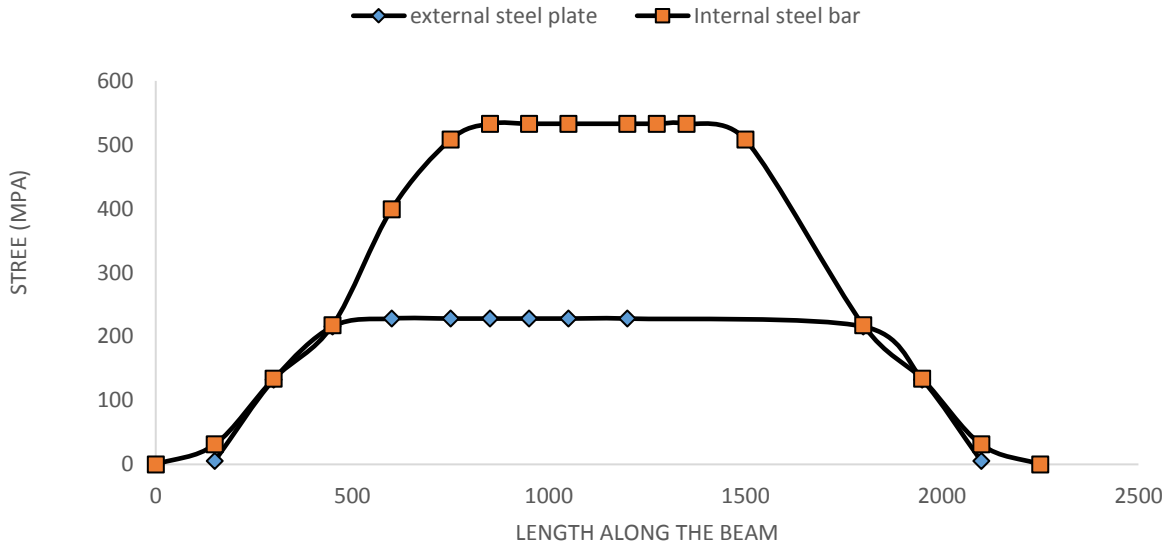

Figure 6. Normal stresses in external plate and internal main steel for beam URB3 at a load of 53 kN

Both materials exhibit a gradual increase in stress from the beam ends toward the midspan, maintaining a paint in the central portion before symmetrically decreasing toward the supports. This behavior suggests that the internal steel bar carries the majority of the tensile load, while the external plate provides additional reinforcement but is less engaged in resisting tension. The difference in stress levels could be attributed to variations in material properties, bond effectiveness, or the load transfer mechanism between the reinforcement and the concrete. The smooth stress transition at the ends indicates effective load distribution, while the plateau regions highlight the sections experiencing near-uniform stress, likely corresponding to areas of maximum bending moment in the beam.

4.0 Conclusions

This study developed and validated a numerical model for predicting the flexural behaviour of reinforced concrete (RC) beams strengthened with externally bonded steel plates. The numerical predictions demonstrated good agreement with experimental results, confirming the reliability of the model in capturing the structural response of plate-bonded RC beams. The model was able to accurately simulate the complete flexural behaviour of strengthened beams up to failure, including load–deflection response, ultimate load capacity, and associated failure patterns.

The results show that the thickness of the externally bonded steel plate plays a significant role in governing beam performance and failure mechanisms. Beams strengthened with relatively thin plates exhibited conventional flexural failure typical of under-reinforced RC beams, whereas increasing the plate thickness led to a transition toward failure modes influenced by the bond behaviour at the plate–concrete interface. This highlights the importance of adequately representing interface interaction in numerical modelling of retrofitted beams.

Furthermore, the inclusion of an external steel plate significantly enhanced beam stiffness and resistance to deformation under applied loads, resulting in improved serviceability performance. An increase in steel plate thickness was also found to produce a corresponding increase in load-carrying capacity, confirming the effectiveness of plate bonding as a strengthening technique for RC beams.

The developed numerical model provides a reliable and efficient analytical tool for evaluating the flexural performance, deformation characteristics, and failure behaviour of plate-bonded RC beams. The model can support the optimization of retrofitting designs and contribute to improved safety and durability of reinforced concrete structures.

References

Al Nuaimi, N., Sohail, M. G., Hawileh, R., Abdalla, J. A., &Douier, K. (2021). Durability of reinforced concrete beams externally strengthened with CFRP laminates under harsh climatic conditions. *Journal of Composites for Construction*, 25(2), 04021005.

Amini Pishro, A., Zhang, S., Zhang, Z., Zhao, Y., Amini Pishro, M., Zhang, L.,& Postel, V. (2022). Structural behavior of FRP-retrofitted RC beams under combined torsion and bending. *Materials*, 15(9), 3213.

Askar, M. K., Hassan, A. F., & Al-Kamaki, Y. S. (2022). Flexural and shear strengthening of reinforced concrete beams using FRP composites: A state of the art. *Case Studies in Construction Materials*, 17, e01189.

Bahraq, A. A., Al-Osta, M. A., Khan, M. I., & Ahmad, S. (2021). Numerical and analytical modeling of seismic behavior of beam-column joints retrofitted with ultra-high performance fiber reinforced concrete. *In Structures* (Vol. 32, pp. 1986-2003). Elsevier.

Bimal, B. A., & Hiroshi M., (2002). Numerical simulation of steel-plate strengthened concrete beam by a nonlinear finite element method model. *Construction and Building Materials* vol 16 pp. 291–301

Cao, X. Y., Shen, D., Feng, D. C., Wang, C. L., Qu, Z., & Wu, G. (2022). Seismic retrofitting of existing frame buildings through externally attached sub-structures: State of the art review and future perspectives. *Journal of building engineering*, 57, 104904.

Dooshabi, A., &Najafgholipour, M. A. (2024). Nonlinear finite element analysis of shear defective reinforced concrete beam to column connections strengthened with three practical techniques. *Engineering Failure Analysis*, 108535.

Firoozi, A. A., Tshambane, M., Firoozi, A. A., & Sheikh, S. M. (2024). Strategic load management: Enhancing eco-efficiency in mining operations through automated technologies. Results in Engineering, 102890.

Goswami, A., & Adhikary, S. D. (2019). Retrofitting materials for enhanced blast performance of Structures: Recent advancement and challenges ahead. *Construction and Building Materials*, 204, 224-243.

Hassan, A., Aldhafairi, F., Abd-EL-Hafez, L. M., &Abouelezz, A. E. Y. (2019). Retrofitting of different types of reinforced concrete beams after exposed to elevated temperature. *Engineering Structures*, 194, 420-430.

Heidarzadeh, G. (2022). *Numerical modelling of bond behaviour of FRP bar reinforced concrete beam under high strain rate impact load* (Doctoral dissertation, City, University of London).

Hu, J. Y., Zhang, S. S., Chen, E., & Li, W. G. (2022). A review on corrosion detection and protection of existing reinforced concrete (RC) structures. *Construction and Building Materials*, 325, 126718.

Irandegani, M. A., Zhang, D., & Shadabfar, M. (2022). Probabilistic assessment of axial load-carrying capacity of FRCM-strengthened concrete columns using artificial neural network and Monte Carlo simulation. *Case Studies in Construction Materials*, 17, e01248.

John, A. T., Osuji S. O., & Nwankwo E. (2022) U-Wrapped Configuration Variation on Shear Strengthening of RC Beam by Carbon Fiber Reinforced Polymer Fabric. Advances *in Engineering Design Technology* 4(3) 2022 pp. 21-30

Jones, R., Swamy, R. N., & Ang, T. H. (1982), "Under- and Over-reinforced Concrete Beams with Glued Steel Plates", The International Journal of Cement Composites and Lightweight Concrete, 4(1), pp 19-32

Mukhopadhyaya, P. & Swarny, R. N. (2001). "Interface shear stress: A new criterion for plate debonding. *Journal of composites for construction*, 5(l). pp 35-43

Omar, M. A. Z. B. (2023). Flexural Strength of Plain Concrete Beam Strengthened With Woven Kenaf FRP Plate: Experimental Works and Numerical Modelling (Doctoral dissertation, Universiti Tun Hussein Onn (Malaysia)).

Raza, S., Khan, M. K., Menegon, S. J., Tsang, H. H., & Wilson, J. L. (2019). Strengthening and repair of reinforced concrete columns by jacketing: State-of-the-artreview. Sustainability, 11(11), 3208.

Rezaee, S., Tavakkoli, M., Doherty, R., & Vargas, F. M. (2020). A new experimental method for a fast and reliable quantification of saturates, aromatics, resins, and asphaltenes in crude oils. *Petroleum Science and Technology*, 38(21), 955-961.

Rincon, L. F., Moscoso, Y. M., Hamami, A. E. A., Matos, J. C., & Bastidas-Arteaga, E. (2024). Degradation Models and Maintenance Strategies for Reinforced Concrete Structures in Coastal Environments under Climate Change: A Review. Buildings, 14(3), 562.

Sano M. (1996) A study of strengthening design of concrete structures using steel plate bonding. Ph.D. Thesis. Tohoku University, Japan, 1996. (in Japanese).

Sara-Simon, S., Kafle, B., & Al-Ameri, R. (2024). A Critical Review of Cold-Formed Steel Built-Up Composite Columns with Geopolymer Concrete Infill. *Journal of Composites Science*, 8(7), 238.

Siddika, A., Al Mamun, M. A., Ferdous, W., & Alyousef, R. (2020). Performances, challenges and opportunities in strengthening reinforced concrete structures by using FRPs–A state-of-the-art review. *Engineering Failure Analysis*, 111, 104480.

Vu, H. D., & Phan, D. N. (2022). A framework for predicting the debonding failure modes of RC beams strengthened flexural with FRP sheets. *Innovative Infrastructure Solutions*, 7(5), 292.

Ziraba, Y. N. & Baluch, M. H. (1995), Computational Model for Reinforced Concrete Beams Strengthened by Epoxy Bonded Steel Plates. *Finite Elements in Analysis and Design*, 20, pp 253-271.

Cite this article as:

Francis, E. W., Auta, S.M., Aguwa J.I. and Abdullahi, A (2025). Numerical Model for Predicting the Flexural Performance of Plate-Bonded Retrofitted RC Beams. *Nigerian Journal of Environmental Sciences and Technology*, 9(2), pp. 138-148. https://doi.org/10.36263/nijest.2025.02.68